2018

Morphology control towards bright and stable inorganic halide perovskite light-emitting diodes

Fangming Jin
Chinese Academy of Sciences

Bo Zhao
Taiyuan University of Technology, zhaobo01@tyut.edu.cn

Bei Chu
Chinese Academy of Sciences

Haifeng Zhao
Chinese Academy of Sciences

Zisheng Su
Chinese Academy of Sciences, suzs@ciomp.ac.cn

See next page for additional authors

Morphology control towards bright and stable inorganic halide perovskite light-emitting diodes

Fangming Jin,[a] Bo Zhao,[b,d*] Bei Chu,[a] Haifeng Zhao,[a] Zisheng Su,[a,c*] Wenlian Li[a] and Furong Zhu[d*]

[a]State Key Laboratory of Luminescence and Applications, Changchun Institute of Optics, Fine Mechanics, and Physics, Chinese Academy of Sciences, Changchun 130033, China

[b]Research Center of Advanced Materials Science and Technology, Taiyuan University of Technology, Taiyuan 030024, China

[c]College of Physics and Information Engineering, Quanzhou Normal University, Quanzhou 362000, China

[d]Department of Physics, Institute of Advance Materials, and Institute of Research and Continuing Education (Shenzhen), Hong Kong Baptist University, Hong Kong, China

*E-mail: zhaobo01@tyut.edu.cn, suzs@ciomp.ac.cn, frzhu@hkbu.edu.hk

ABSTRACT: The effect of morphology control on the performance of inorganic cesium lead halide based green perovskite light-emitting diodes (PeLEDs) was analyzed. The PeLEDs were prepared using two different formulation approaches: (1) the solution was prepared by dissolving $CsPbBr_3$ powders in dimethyl sulfoxide (DMSO), and (2) the precursor solution was formulated by dissolving CsBr and $PbBr_2$ powders with different molar ratios CsBr to $PbBr_2$ in DMSO. The peak luminance of 4590 cd/m^2 was obtained for PeLEDs made with $CsPbBr_3$-solution, which is 48 and 12 times higher than that of the optimized PeLEDs fabricated using $CsBr/PbBr_2$ precursor solutions with different molar ratios of CsBr to $PbBr_2$ of 2:1 and 1:1. Our results reveal that the morphology and excess interstitial Pb atoms in the perovskite

emitting layer play the important role in modulating the current losses and radiative decay rate, which were optimized in this work for attaining efficient operation of the PeLEDs.

Keywords: inorganic halide perovskite, light-emitting diodes, morphology control

1. Introduction

Recently organic-inorganic hybrid perovskite has attracted increasing attention for application in photovoltaic devices due to its low cost, earth-abundance and solution-fabrication process at low temperature under ambient condition. Rapid progresses haven been made in perovskite solar cells with power conversion efficiency of above 20%.[1-4] Organic-inorganic hybrid perovskites also are emerging as a promising technology for use in light-emitting diodes (LEDs) because they can provide high color purity with full width at half maximum (FWHM) of ~20 nm irrespective of their crystal size. Unlike the conventional inorganic quantum dots, their intrinsic crystal structure is like a multiple quantum well.[5-10] The perovskite nanoparticles have a high photoluminescence quantum yield (PLQY). The reports on the progresses of organic-inorganic hybrid perovskite LEDs increased rapidly in less than one year, e.g., the bilayer perovskite light-emitting diodes (PeLEDs) with a high current efficiency of 42.9 cd/A were demonstrated.[11] More recently, LEDs based on all solution-processable inorganic perovskites also attracted considerable research interests because of the advantages of high PLQY, easy tunable emission colors, and high color purity for applications in solid state lighting and displays. [12-15] The solution-processed inorganic $CsPbBr_3$-based perovskite LEDs, fabricated using CsBr-$PbBr_2$ precursor solutions with two different CsBr/$PbBr_2$ molar ratios of 2:1 and 1:1, with maximum luminance of 407 cd/m^2 and 132 cd/m^2 were demonstrated.[12] The performance of $CsPbBr_3$-based PeLEDs remains modest, due to the incomplete surface coverage of

perovskite films and the exciton quenching caused by the excess interstitial Pb atoms. The presence of the excess Pb atoms deteriorates the luminance because of the increase in nonradiactive decay rate, and thereby causing decrease in the radiative decay rate.[16] The existence of interstitial Pb atoms in pure inorganic perovskite is more severe than that in organic-inorganic hybrid perovskite, due to the lower solubility of CsBr than that of the methylammonium halide (MABr) in solution. Interstitial Pb atoms can emerge in $MAPbBr_3$ even if MABr and $PbBr_2$ are mixed in a molar ratio of 1:1 because of the unintended losses of Br atoms or the incomplete reaction between MABr and $PbBr_2$.[17] In a pure inorganic perovskite, stoichiometric ratio of CsBr to $PbBr_2$ is less than 1:1 because of the low solubility of CsBr in solvents such as dimethylformamide (DMF) or dimethyl sulfoxide (DMSO), leading to a much more excess of interstitial Pb atoms in the perovskite layer. Simultaneous reduction of the concentrations of $PbBr_2$ and CsBr seems an effective method to decrease the ratio of $PbBr_2$ to CsBr in the perovskite. However, reducing the concentrations of precursors in the formulations results in inevitably a decrease in the perovskite layer thickness, a poorer surface coverage of perovskite film, and thereby a smaller photocurrent. These are two limiting factors and remain as the open challenge for further improvement in the performance of inorganic perovskite-based PeLEDs.

In this work, the effect of morphology and presence of interstitial Pb atoms on the performance of inorganic cesium lead halide perovskite based green PeLEDs was analyzed. Our results reveal that the morphology of the perovskite film and amount of interstitial lead atoms relate closely the efficient operation of PeLEDs, which can be controlled by adjusting the perovskite precursor solution. Morphology control provides an optimal coverage and effectively

blocking of pinholes or electrical shunting paths with a smaller perovskite crystal. The formation of interstitial Pb atoms, which is closely associated with the strong exciton quenching, can be suppressed by optimizing the perovskite precursor solution. PeLEDs with low current losses and higher radiative decay rate were attained by morphology control and suppression of interstitial Pb atoms in the perovskite light-emitting layer, approaching a peak brightness of 4590 cd/m^2, which is 11 times higher than that reported for the similar PeLEDs[12], and also is 48 and 12 times higher than reference devices made with CsBr/$PbBr_2$ precursor solutions having different molar ratios of 2:1 and 1:1.

2. Experimental Section

2.1 Synthesis of $CsPbBr_3$ powders: The $CsPbBr_3$ powders were synthesized following the procedure reported in the literature.[18] Firstly, the $PbBr_2$ powers (7.31 g, 20 mmol) were dissolved in 30 ml of 48% aqueous HBr to form a pale-yellow solution. Secondly, the CsBr (4.26 g, 20 mmol) powders were dissolved in 10 ml of H_2O. The precipitation of a bright orange solid appeared by mixing the $PbBr_2$ and CsBr solutions. Finally, the solid was suction filtered, washed copiously with absolute EtOH and dried under vacuum to obtain >10 g of pure $CsPbBr_3$ powders, with a yield of >90%. The X-ray diffraction (XRD) patterns and photograph taken for the $CsPbBr_3$ powders thus synthesized are shown in Fig. S1.

2.2 Device Fabrication: All the materials used for the device fabrication were purchased from the commercial sources and used without further purification except for the $CsPbBr_3$ powders which were synthesized in-house in this work. Indium tin oxide (ITO)-coated glass substrates with a sheet resistance (Rs) of 15 Ω/sq were cleaned by ultra-sonication in acetone,

detergent, and acetone, and the ITO/glass substrates were then exposed to ultraviolet zone for 10 min prior to the device fabrication. PEDOT:PSS was spin-coated onto ITO/glass at a rotation speed of 3500 rpm for 50s, and annealed in air at 120 °C for 20 min. 200-nm thick $CsPbBr_3$ perovskite films were formed on PEDOT:PSS using different $CsPbBr_3$ solutions, e.g., solution A (dissolving 0.55 M $CsPbBr_3$ in DMSO), solution B (filtered solution with a molar ratio of CsBr to $PbBr_2$ 1:1 in DMSO) and solution C (filtered solution with a molar ratio of CsBr to $PbBr_2$ 2:1in DMSO), by spin-coating at a rotation speed of 1500 rpm for 70 s. A 5 wt% 4,7-diphenyl-1,10-phenanthroline (BPhen) in chloroform was dropped immediately on the surface of the $CsPbBr_3$ perovskite film for 30 s to reduce the crystal size. The samples were then baked at 90 °C for 10 min and transferred into a high-vacuum chamber (with a base pressure of ~3×10^{-4} Pa) for preparation of 50-nm thick BPhen and 80-nm thick Ag (80 nm) bilayer contact sequentially by thermal deposition at deposition rates of 1 and 3 Å/s, respectively.

2.3 Characterization: The current density-voltage-luminance characteristics of the PeLEDs were measured using a Keithley model 2400 power supply combined with a ST-900M spot photometer, and were recorded simultaneously during the measurements. Absorption spectra of the perovskite layers were measured using a Shimadzu UV-3101PC spectrophotometer. Steady-state photoluminescent (PL) spectra of the perovskite films were measured using a Hitachi F7000 fluorescence spectrophotometer. The electroluminescent (EL) spectra of the PeLEDs were measured using an OPT-2000 spectrophotometer. Scanning electron microscopy (SEM) images of the perovskite layers were obtained using a Hitachi S4800 field emission scanning electron microscope. XRD patterns of the perovskite films were recorded with a Rigaku D/Max-2500 diffractometer using Cu Kαradiation (λ=1.54 Å). The PeLEDs were not

encapsulated and were measured in air at room temperature.

3. Results and Discussion

The PeLEDs have a multilayer structure of ITO/PEDOT:PSS (~40 nm)/$CsPbBr_3$ (~200 nm)/BPhen (50 nm)/silver (Ag 80 nm), the schematic cross-sectional view of the PeLEDs is showed in Fig. 1a. The corresponding schematic flat-band energy level diagram of the devices is showed in Fig. 1b. The 50-nm thick wide bandgap BPhen layer was employed serving as an electron transporting layer and a hole blocking layer, because of its excellent optical transparency and a shallow conduction-band energy level. While the PEDOT:PSS was used as a hole transporting layer and electron blocking layer. Three types of PeLEDs, defined as Device-A, Device-B and Device-C, were prepared using different $CsPbBr_3$ formulation solutions, e.g., "Device-A" type PeLEDs were fabricated using perovskite solution formulated by dissolving 0.55M synthesized $CsPbBr_3$ powders in DMSO (Precursor-A). The $CsPbBr_3$ powders can be dissolved sufficiently in DMSO forming a clear and transparent solution after annealing at 70 ^{O}C for 20 min. "Device-B" and "Device-C" types PeLEDs were fabricated using presursor solutions formulated by blending CsBr and $PbBr_2$ in DMSO with different molar ratios of 1:1 (Precursor-B) and 2:1 (Precursor-C). Due to the inferior solubility of CsBr, precipitates were formed in both Precursor-B and Precursor-C precursor solutions. The photo pictures taken for different perovskite formulation solutions of precursor-A, Precursor-B and Precursor-C are shown in Fig. S2, showing that Precursor B has a pale-yellow color and Precursor-C has a yellowish color due to the presence of excess interstitial Pb atoms in $CsPbBr_3$ solution, suggesting the stoichiometric ratio of CsBr to $PbBr_2$ in the precursor solution is less than 1:1.

The cross-sectional SEM images measured for the perovskite layers on PEDOT:PSS fabricated by different perovskite formulation solutions of precursor-A, Precursor-B and Precursor-C are presented in Fig. S3. These $CsPbBr_3$ samples have a similar layer thickness of about 200 nm, revealing that the concentration of $PbBr_2$ in the solutions dominates the perovskite film thickness. The huge surface roughness comes from the large crystal size, forming voids between the crystals and thereby a low surface coverage. The crystal structures of the $CsPbBr_3$ perovskite films prepared by three different formulations were analyzed using XRD measurements. XRD patterns measured for the perovskite films prepared by three different solutions are given in Fig. S4, revealing that all films consist of polycrystalline $CsPbBr_3$ phase.[18] It can be seen from the XRD patterns that the change in the stoichiometric ratio of CsBr to $PbBr_2$ in the solutions had very little effect on the crystallinity of the resulting $CsPbBr_3$ perovskite films.

UV-vis absorption and PL spectra measured for the $CsPbBr_3$ perovskite film prepared by Precursor-A are showed in Fig. 2a. The absorption peak of the perovskite film locates at 515 nm, while the position of the PL emission peak is at around 532 nm, with a narrow FWHM of 18 nm, agreed with those reported previously for $CsPbBr_3$-based green PeLEDs.[12] While the UV-vis absorption and PL spectra of perovskite films formed using Precursor-B and Precursor-C precursor solutions are similar to that measured for the film papered by Precursor-A solution, as shown in Fig. S5. The non-zero baseline in the absorption spectra can be attributed to light scattering and interference effects. The EL spectra measured for all the perovskite devices are plotted in Fig. 2b. PeLEDs prepared by three different formulation solutions exhibit almost the same emission behavior, which implies that the light-emitting comes from $CsPbBr_3$-based perovskite emitter and no emission from interface material was occurred. The EL peaks located

at 527 nm have a FWHM of 21 nm, which is in little difference with the PL spectra of these $CsPbBr_3$ films.

The SEM images measured for the $CsPbBr_3$ perovskite films prepared by different solutions of Precursor-A, Precursor-B and Precursor-C are showed in Fig. 3. Perovskite layers with micrometer-sized $CsPbBr_3$ domains were scattered in perovskite layers on PEDOT:PSS surface, prepared by Precursor-B and precursor-C solutions. A large amount of volume remained unfilled because the perovskite layers were not fully occupied by the $CsPbBr_3$ cuboids. This high surface roughness and the formation of pinholes in inorganic halide perovskite films result in the formation of a poor interface with the electron transport layer forming electrical shunt paths, which limit severely the current efficiency in PeLEDs. In contrast, for $CsPbBr_3$ perovskite film prepared by Precursor-A solution, a perfect surface coverage was obtained and the $CsPbBr_3$ crystal morphology changed to a well-packed assembly of tiny grains ranging from 100 to 250 nm, as shown in Fig. 3a and 3d. The smaller grains can limit spatially the diffusion length of excitons and reduce the possibility of exciton dissociation into carriers. A 95% coverage of the $CsPbBr_3$ perovskite was obtained for film prepared by Precursor-A solution, estimated based on SEM images using Image J Software, which is much higher than that of the films prepared by Precursor-B solution (≈80%) and Precursor-C solution (≈70%). The pinholes in the perovskite films caused by incomplete surface coverage lead to substantial nonradiative current losses. We propose that the difference in the morphology of the perovskite films fabricated with different precursor solutions originates from different stoichiometric ratios of CsBr to $PbBr_2$ in the films, where an excess $PbBr_2$ seems to be in favor of large crystal formation in the film growth progress.[19]

The current density-voltage-luminance characteristics of the PeLEDs are presented in Fig. 4a. The EL performance of the PeLEDs is summarized in Table 1. It shows that the optimal morphology improves the crystallization quality and helps to improve the conductivity, contributing to a significant improvement in current density of Device-A, agreeing with the phenomenon reported previously.[12] The reference devices of "Device-B" and "Device-C" PeLEDs had a maximum luminance of 92 cd/m^2 and 337 cd/m^2, respectively, similar to a maximum luminance of 132 cd/m^2 reported for the device made with a molar ratio of CsBr to $PbBr_2$ of 1:1 in the precursor solution and a maximum luminance of 407 cd/m^2 for PeLED fabricated with a molar ratio of CsBr to $PbBr_2$ of 2:1. "Device-A" type PeLEDs had the lowest turn-on voltage of 2.8 V as compared to 4.2 V for Device-B and 3.7 V for Device-C. Notably, pure green emission can be observed from Device-A at an operating voltage as low as 2.8 V, indicating that an efficient charge injection into the $CsPbBr_3$ perovskite emitting layer was achieved. In the present experiments, an increased current efficiency and external quantum efficiency (EQE) were observed with both increased voltage and current density, which showed in Fig. 4b. The current efficiency and EQE of the green PeLEDs rise with increase in current density due to a dominant radiative bimolecular recombination at the higher excitation densities. The EQE of the best-performing "Device-A" type PeLED reaches up to ≈0.06% at the highest luminance of 4590 cd/m^2 with a current density of 1830 mA/cm^2, where a highest current efficiency of 0.25 cd/A is also achieved. The maximum luminance, current efficiency and EQE of Device-A are 48, 28 and 29 times higher than those measured for Device-B, and 12, 21 and 19 times higher than those of Device-C. It was reported that a reduced trap density was account for the improved performance of PeLEDs fabricated using a CsBr-rich solution.[12] We show here

that this is not the whole reasons. Compared to CsBr-rich film, there exist much more pinholes in the perovskite film fabricated by the equimolar CsBr-$PbBr_2$ solution as shown in the SEM images. The poor coverage of the film fabricated by the equimolar CsBr-$PbBr_2$ solution must result in a large amount of electrical shunting paths and induce serious current losses, which lead to inferior device performances in luminance, current efficiency and EQE. We also found that that breakdown is much easier for Device-B and Device-C than Device-A at the same current density, which is attributed to the local Joule heating from the high current filament through the pinholes. This is accordance with the device working lifetime test. As shown in Fig. 5, the emission from a non-encapsulated Device-A can remain for more than half an hour, while the breakdown in a few seconds was observed for Device-B and Device-C types of PeLEDs. Hence, the pinholes in the perovskite films limit the device EQE through nonradiative current losses, as well as limit the maximum brightness of the PeLEDs by causing early breakdown at low bias voltages. This aside, the number of excess interstitial Pb atoms is much lower in Device-A as compared to that in Device-B due to the poor solubility of CsBr in the precursor solution, as shown in Fig. S2. Relatively lower density of the excess interstitial Pb atoms in Device-A reduces the exciton quenching probability, which is beneficial for promoting radiative recombination processes, and thereby enhancing luminescent efficiency eventually.

The EL spectra of a “Device-A” type PeLED at different drive voltages are shown in Fig. 6a, indicating that the EL spectra of the PeLED are not dependent on the external bias. The device gives a very narrow EL spectrum, arising from the band-edge emission. The PeLEDs displays the EL spectra solely from $CsPbBr_3$ without any noticeable contribution from any charge transport materials, indicating that the $CsPbBr_3$ emitter serves as the primary exciton

recombination zone during device operation. The corresponding Commission Internationale de l'Eclairage (CIE) color coordinates of (0.16, 0.78) for the PeLEDs are shown in Fig. 6b, satisfying the requirement of the CIE coordinates for application in displays. Inset of Fig. 6b shows the photograph taken for a Device-A emitting pleasant green light, showing the uniform emission across the entire device pixel, demonstrating that the emission quality and the potential of the $CsPbBr_3$–based PeLEDs made with a solution-fabrication process.

It is necessary to note that device performance can be further optimized by the interface engineering such as replacing the charge transfer layer of PEDOT:PSS. The high hole injection barrier exist at the PEDOT:PSS/perovskite interface because of the mismatch between the ionization potential (IP) level of the perovskite (~6.0 eV) and the work function (WF) of PEDOT:PSS (ca. 5.2 eV). This large hole injection barrier (~0.8 eV) limits hole injection into perovskite layer and hence the overall electron-hole current balance in the emitting layer (EML). PEDOT:PSS hole transporting layer also induces significant exciton quenching at the PEDOT:PSS/$CsPbBr_3$ interface because of the long exciton diffusion length in the perovskite layer, and thereby reduces the device efficiency by limiting the radiative recombination of charge carriers.[20,21] Therefore, using a high-WF hole injection material enables to prevent exciton quenching in PeLEDs, which is of prime importance to achieve high EL performance by a combination of removing a high hole injection barrier and suppressing luminescence quenching. It was found that there existed an unintended loss of Br atoms in the perovskite layers, e.g., the molar ratio of CsBr to $PbBr_2$ is less than 1:1 even in the perovskite films prepared by Precursor-A solutions. The excess Pb interstitial atoms would induce strong exciton quenching. In the organic-inorganic hybrid perovskite LEDs, the maximum current efficiency

can be varied from 4.87×10^{-2} to 21.4 cd/A by increasing the molar ratio of CH_3NHBr_3 to $PbBr_2$ from 1:1.05 to 1.05:1.[11] It is anticipated that the performance of the PeLEDs developed in this work can be further improved by introducing a small amount of CsBr in the Precursor-A solution. The analyses made with the device performance and the morphological characterizations suggest that the $CsPbBr_3$ film prepared by Precursor-A solution provides smaller crystalline grain and optimal surface coverage, which effectively preventing the formation of pinholes or electrical shunting paths, and suppression of the excess interstitial Pb atoms. The combined effects avoid the low current and losses to the nonradiative decay leading to a significant enhancement in device efficiency.

4. Conclusion

In summary, the performance of inorganic cesium lead halide perovskite based green PeLEDs was analyzed. We found that the smooth morphology and the reduction of the excess interstitial Pb atoms in the perovskite emitter play an important role for efficient operation of PeLEDs. The quality of the perovskite emitter was controlled by optimizing the formulation of the perovskite precursor solution. Morphology and the excess interstitial Pb atoms are closely associated with the surface coverage of the perovskite emitter, which was optimized for preventing the formation of pinholes, electrical shunting paths and low current losses. The remarkable improvement in the EL performance of solution-processed PeLEDs was demonstrated. The outcomes of this work offer an attractive option toward low cost and solution-processable inorganic PeLEDs for applications in large-area displays and solid-state lighting.

Acknowledgements

This work was supported by the National Natural Science Foundation of China (Grants. 61604149, 61376062, 61376022, 61575192 and 61504145); The Science and Technology Development Plan of Jilin Province (20170520130JH and 20140101094JC); The Project of Jiangsu Key Laboratory for Carbon-Based Functional Materials and Devices (KJS1615). Hong Kong Baptist University Faculty Research Grant (FRG2/2016-17/088); Interinstitutional Collaborative Research Scheme (RC-ICRS/15-16/04); and Shenzhen Peacock Plan (KQTD20140630110339343).

References

1. J. Burschka, N. Pellet, S. J. Moon, R. H. Baker, P. Gao, M. K. Nazeeruddin and M. Gratzel, *Nature*, 2013, **499**, 316.
2. H. S. Kim, C. R. Lee, J. H. Im, K. B. Lee, T. Moehl, A. Marchioro, S. J. Moon, R. H. Baker, J. H. Yum, J. E. Moser, M. Gratzel and N. G. Park, *Sci. Rep.*, 2012, **2**, 591.
3. M. M. Lee, J. Teuscher, T. Miyasaka, T. N. Murakami and H. J. Snaith, *Science*, 2012, **338**, 643.
4. H. Zhou, Q. Chen, G. Li, S. Luo, T. B. Song, H. S. Duan, Z. Hong, J. You, Y. Liu and Y. Yang, *Science*, 2014, **345**, 542.
5. V. D'Innocenzo, A. R. Srimath Kandada, M. D. Bastiani, M. Gandini and A. Petrozza, *J. Am. Chem. Soc.*, 2014, **136**, 17730.
6. R. L. Hoye, M. R. Chua, K. P. Musselman, G. Li, M. L. Lai, Z. K. Tan, N. C. Greenham, J. L. MacManus-Driscoll, R. H. Friend and D. Credgington, *Adv. Mater.*, 2015, **27**, 1414.

7. Y. H. Kim, H. Cho, J. H. Heo, T. S. Kim, N. Myoung, C. L. Lee, S. H. Im and T. W. Lee, *Adv. Mater.*, 2015, **27**, 1248.
8. G. Li, Z. K. Tan, D. Di, M. L. Lai, L. Jiang, J. H. Lim, R. H. Friend and N. C. Greenham, *Nano lett.*, 2015, **15**, 2640.
9. J. Li, S. G. Bade, X. Shan and Z. Yu, *Adv. Mater.*, 2015, **27**, 5196.
10. J. Wang, N. Wang, Y. Jin, J. Si, Z. K. Tan, H. Du, L. Cheng, X. Dai, S. Bai, H. He, Z. Ye, M. L. Lai, R. H. Friend and W. Huang, *Adv. Mater.*, 2015, **27**, 2311.
11. H. Cho, S. H. Jeong, M. H. Park, Y. H. Kim, C. Wolf, C. L. Lee, J. H. Heo, A. Sadhanala, N. Myoung, S. Yoo, S. H. Im, R. H. Friend and T. W. Lee, *Science*, 2015, **350**, 1222.
12. N. Yantara, S. Bhaumik, F. Yan, D. Sabba, H. A. Dewi, N. Mathews, P. P. Boix, H. V. Demir and S. Mhaisalkar, *J. Phys. Chem. Lett.*, 2015, **6**, 4360.
13. X. Zhang, H. Lin, H. Huang, C. Reckmeier, Y. Zhang, W. C. Choy and A. L. Rogach, *Nano lett.*, 2016, **16**, 1415.
14. J. Song, J. Li, X. Li, L. Xu, Y. Dong and H. Zeng, *Adv. Mater.*, 2015, **27**, 7162.
15. L. Protesescu, S. Yakunin, M. I. Bodnarchuk, F. Krieg, R. Caputo, C. H. Hendon, R. X. Yang, A. Walsh and M. V. Kovalenko, *Nano lett.*, 2015, **15**, 3692.
16. E. Dulkeith, M. Ringler, T. A. Klar, J. Feldmann, A. M. Javier and W. J. Parak, *Nano lett.*, 2005, **5**, 585.
17. R. Sheng, A. H. Baillie, S. Huang, S. Chen, X. Wen, X. Hao and M. A. Green, *J. Phys. Chem. C*, 2015, **119**, 3545.
18. C. C. Stoumpos, C. D. Malliakas, J. A. Peters, Z. Liu, M. Sebastian, J. Im, T. C. Chasapis, A. C. Wibowo, D. Y. Chung, A. J. Freeman, B. W. Wessels and M. G. Kanatzidis, *Cryst.*

Growth Des., 2013, **13**, 2722.

19. H. S. Jung and N. G. Park, *Small*, 2015, **11**, 10.
20. S. D. Stranks, G. E. Eperon, G. Grancini, C. Menelaou, M. J. Alcocer, T. Leijtens, L. M. Herz, A. Petrozza and H. J. Snaith, *Science*, 2013, **342**, 341.
21. G. Xing, N. Mathews, S. Sun, S. S. Lim, Y. M. Lam, M. Gratzel, S. Mhaisalkar and T. C. Sum, *Science*, 2013, **342**, 344.

Table 1 A summary of the performance of different PeLEDs.

Samples	**$V_{turn\text{-}on}$ (V)**	**L_{max}(cd/m^2)**	**Current efficiency (cd/A)**	**EQE_{max} (%)**
Device-A	2.8	4590	0.25	0.06
Device-B	4.2	92	0.0085	0.002
Device-C	3.7	337	0.011	0.003

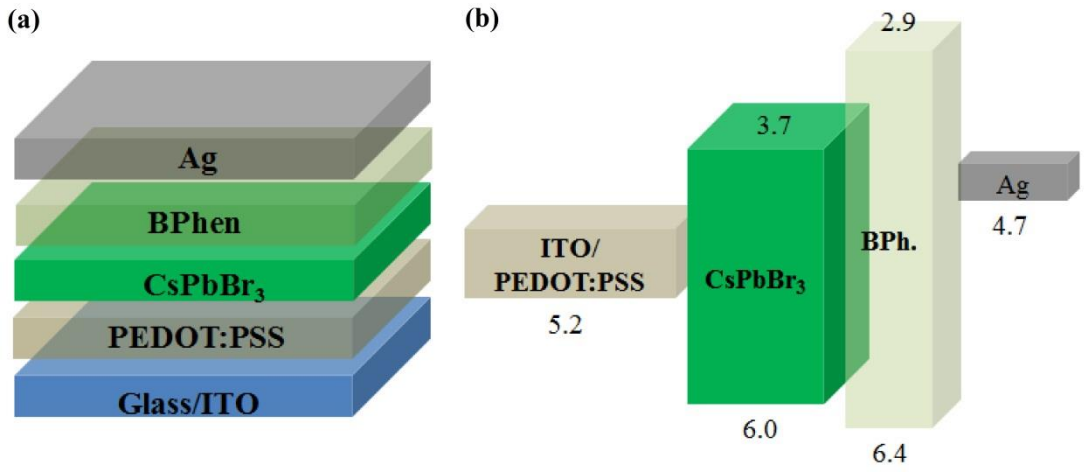

Fig. 1 (a) Schematic cross-sectional view and (b) schematic energy level diagram of the PeLED

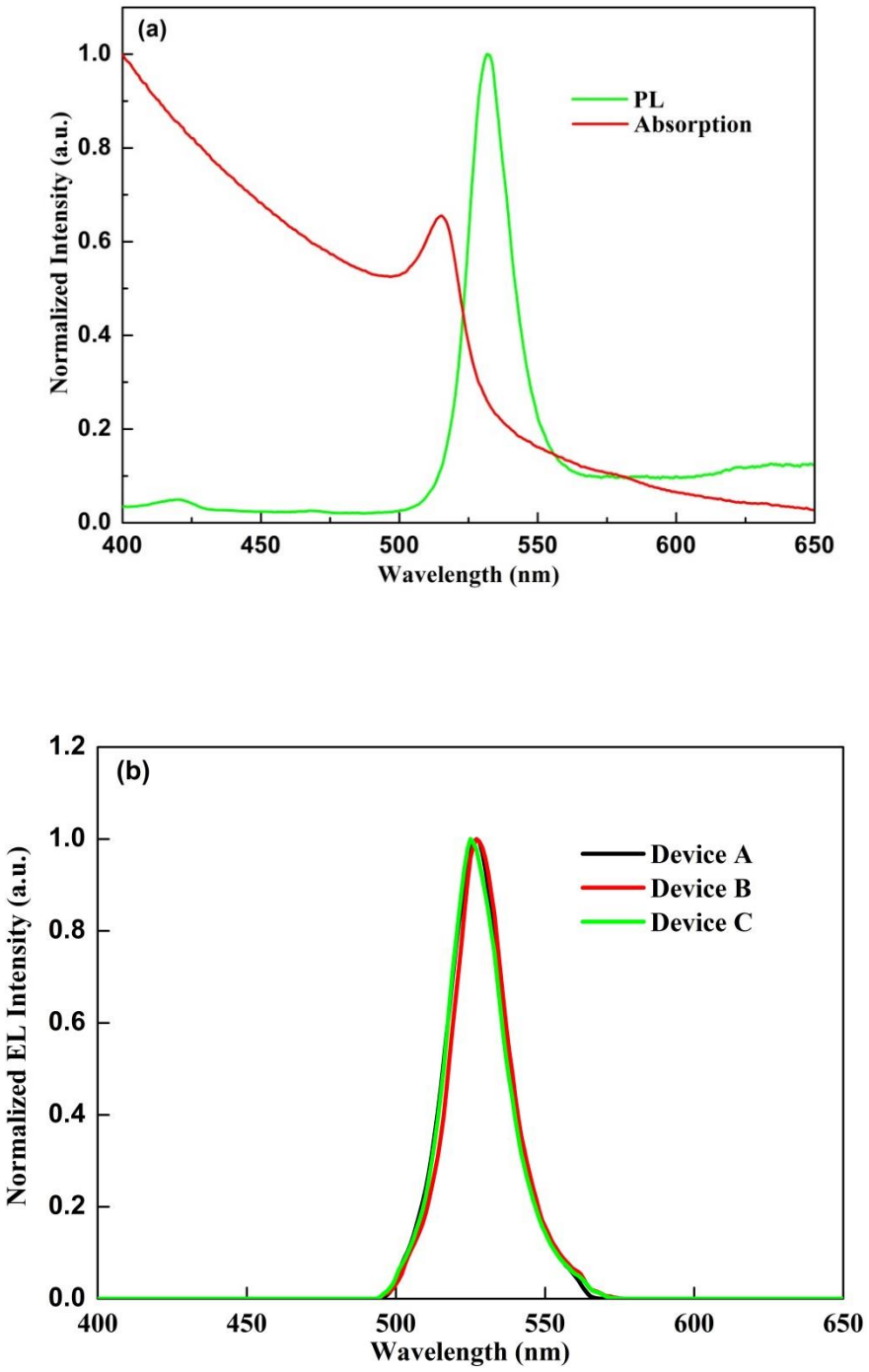

Fig. 2 (a) Absorption and PL spectra measured for the perovskite film prepared using precursor-A solution (365 nm excitation wavelength). (b) Normalized EL spectra measured for PeLEDs prepared by different perovskite formulation solutions of Precursor-A, Precursor-B and Precursor-C.

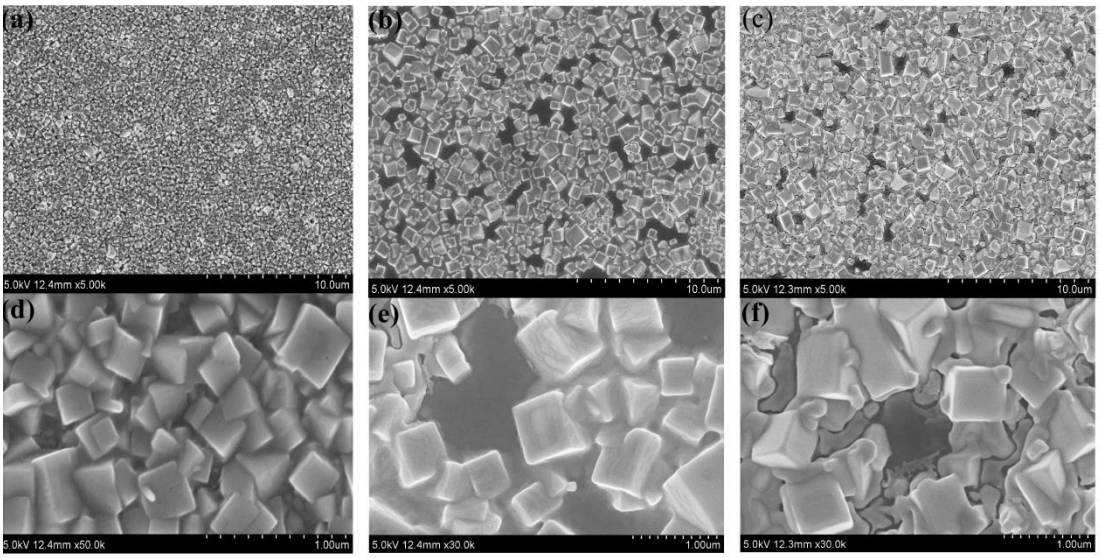

Fig. 3 The SEM images measured for $CsPbBr_3$ perovskite films prepared by different formulation solutions of Precursor-A, (a) and (d), Precursor-B (b) and (e), and Precursor-C (c) and (f).

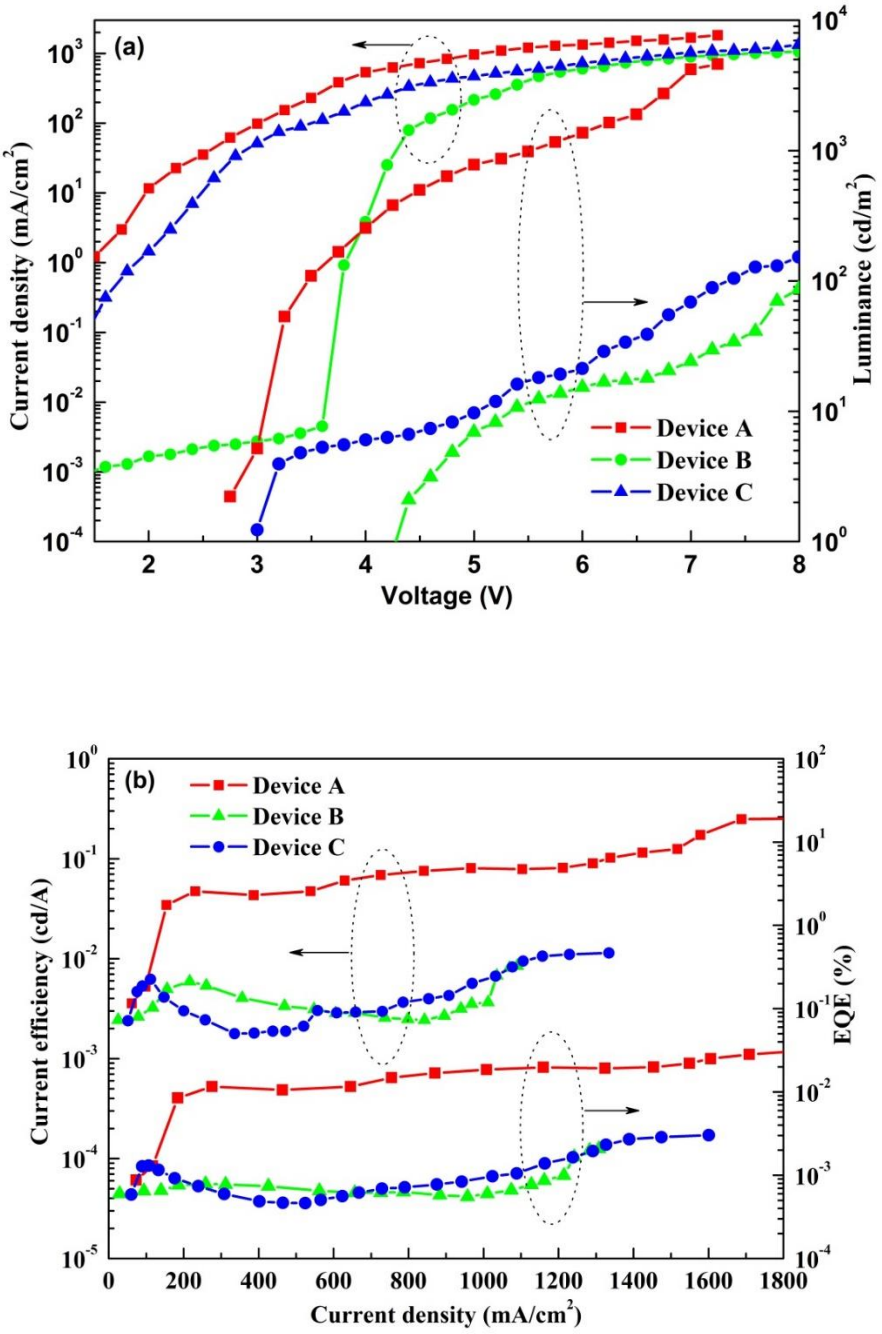

Fig. 4 (a) Current density-voltage-luminance characteristics, (b) current efficiency-current density-EQE characteristics measured for three types of PeLEDs prepared using different formulation solutions of Precursor-A, Precursor-B and Precursor-C.

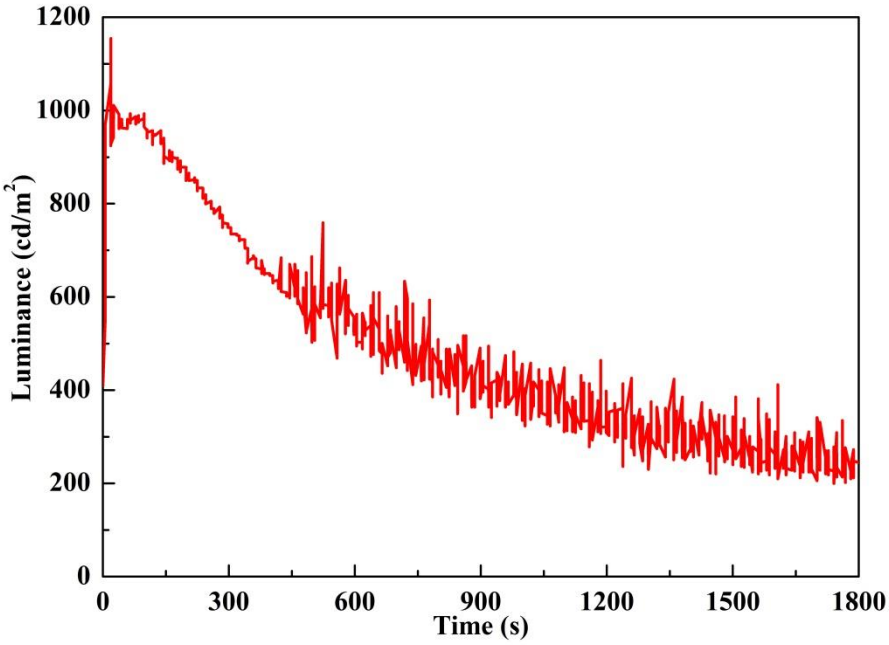

Fig. 5 Luminance-aging time characteristics measured for Device-A type PeLED under a constant operation voltage of 6 V.

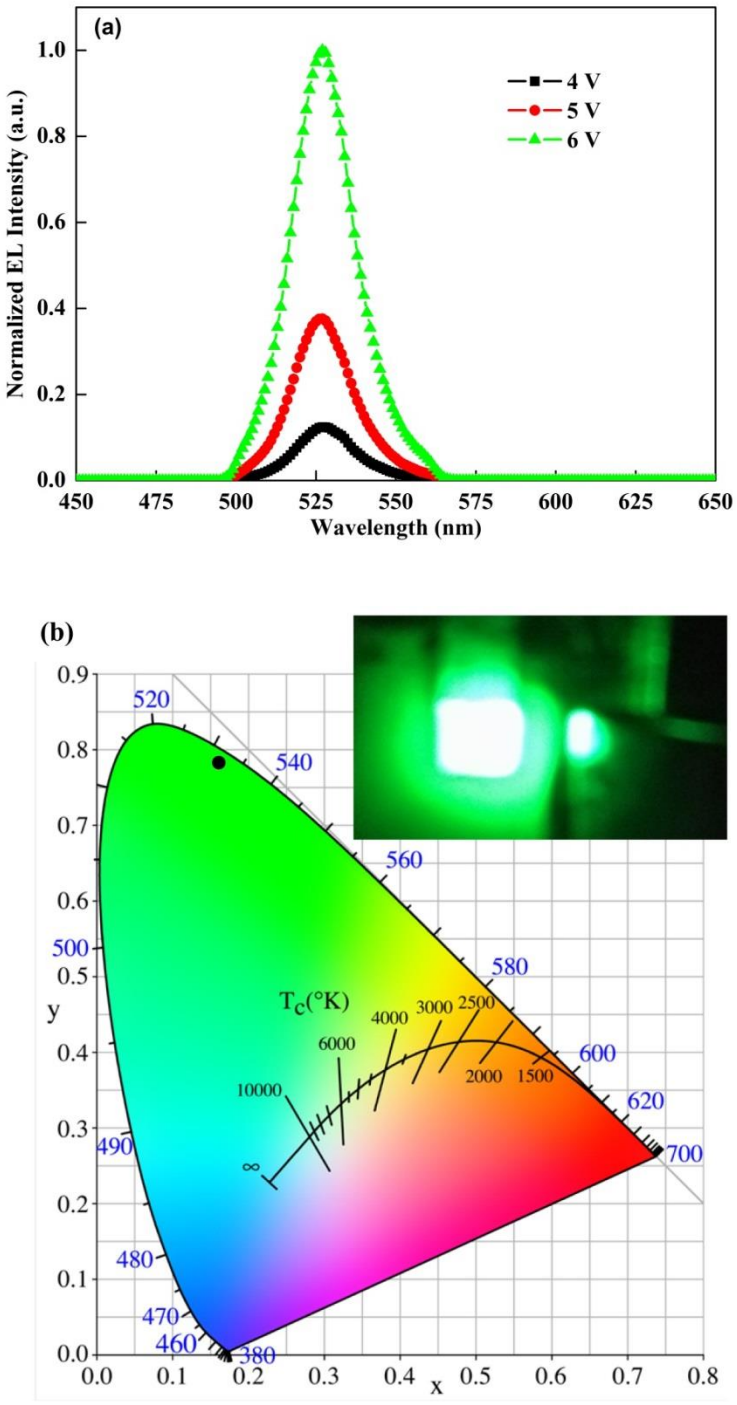

Fig. 6 (a) The EL spectra measured for Device-A type PeLED at different driving voltages of 4 V, 5 V and 6 V. (b) The CIE coordinates for the EL spectrum of Device-A operated at 6 V. Inset: photo picture taken for a working Device-A emitting green light.